Parallelizing the Keldysh Formalism for Strongly Correlated Electrons

J.K. Freericks and V. Turkowski
Georgetown University, Department of Physics, Washington, DC
{freericks, turk}@physics.georgetown.edu

V. Zlatić
Institute of Physics of the University of Zagreb, Zagreb, Croatia
zlatic@ifs.hr

Abstract

Nonequilibrium quantum mechanics can be solved with the Keldysh formalism, which evolves the quantum mechanical states forward in time in the presence of a time-dependent field, and then evolves them backward in time, undoing the effect of the time-dependent field. The Feynman path integral over the Keldysh contour is employed to calculate the strongly correlated Green's function. We examine the accuracy of this procedure for the simplest problem that requires a nonequilibrium formulation: the electron spectral function of the spinless Falicov-Kimball model.

1. Introduction

Electrons are correlated when the Coulomb repulsion between them is strong enough that it plays a significant role in determining the motion of the electrons through the crystal. Correlated electrons are of interest to the military, because their properties (metallic/insulating/magnetic/superconducting/etc.) can be easily tuned by changing pressure, chemical composition, irradiation with electromagnetic fields, and so on, and form the basis of many so-called smart materials and devices. In addition, a large number of materials of interest to the military (like Plutonium) have strong electron correlations

Our research problem involves understanding strongly correlated materials when they are placed under intense electromagnetic fields that can drive them out of equilibrium creating interesting dynamical and relaxational effects (examples include intense pulsed laser irradiation or interacting with large amplitude microwaves). Our main focus is to the Josephson junction device[1] (a sandwich of a superconductor-barrier-superconductor which has the potential for ultra high speed digital electronics[2]), but the principles can be applied to a large number of different devices. The many-body formalism for nonequilibrium problems is solved by

a Feynman path integral over the so-called Keldysh contour[3,4] which involves an evolution forward in time as the external fields are turned on, evolution out to a long time, then an inverse evolution backward in time where the fields are turned off. Solving the Feynman path integral requires evaluating finite-sized determinants of discretized matrices that represent the continuous matrix operator along the contour. We typically require the determinant of approximately 500 general complex matrices with sizes up to about 2100 × 2100 for a production run. This computational effort is easily parallelized. The numerical solutions suffer from a discretization error that gets worse as the temperature is lowered, and accurate calculations require a careful extrapolation with different discretization sizes to the limit where the discretization goes to zero. Here we benchmark the numerics by solving for the *f*-electron spectral function of the spinless Falicov-Kimball model[5].

The Falicov-Kimball model is the simplest model of electron correlations (and the problem we investigate is the simplest nontrivial Keldysh problem). It possesses two types of electrons: conduction electrons, which can hop to any of their nearest neighbors and localized *(f)* electrons which are localized on the lattice sites. There is a Coulomb repulsion U between conduction electrons and localized electrons on the same lattice site. As U increases, the conduction band splits into two bands with an energy gap in between, and undergoes the so-called Mott metal-insulator transition. In this contribution, we restrict ourselves and all formulas to the case of half filling, where half of the lattice sites are occupied by the conduction electrons and half by the localized electrons. In this case, the Hamiltonian becomes[5]

$$
\mathcal{H} = \frac{t^*}{\sqrt{Z}} \sum_{\langle ij \rangle} \left(c_i^\dagger c_j + c_j^\dagger c_i \right) + U \sum_i c_i^\dagger c_i f_i^\dagger f_i
$$
$$
- \frac{U}{2} \sum_i \left(c_i^\dagger c_i + f_i^\dagger f_i \right), \tag{1}
$$

where $c_i^\dagger$ (c_i) creates (destroys) a conduction electron at site i, $f_i^\dagger$ (f_i) creates (destroys) a localized electron at site i, U is the interaction strength, and t^* is the hopping integral. The symbol Z represents the number of nearest neighbors, and $\langle ij \rangle$ denotes a sum over all nearest neighbor pairs. The first term is the kinetic energy of the conduction electrons, the second term is the Coulomb repulsion, and the third term is the chemical potential times the filling for both electrons.

We solve this problem on an infinite coordination number[6] ($Z \to \infty$) Bethe lattice, which has a noninteracting density of states (DOS) that is a semicircle

$$\rho(\epsilon) = \frac{1}{2\pi t^{*2}} \sqrt{4t^{*2} - \epsilon^2} \ . \qquad (2)$$

The noninteracting bandwidth is $4t^*$. We choose t^* as our energy unit and set it equal to 1. See Reference 7 for a review of the equilibrium and linear response solutions.

2. Formalism

We start with an examination of the retarded local Green's function for the conduction electrons, defined to be

$$G_{jj}(t) = -i\theta(t)\mathbf{Tr}\left\langle e^{-\beta\mathcal{H}}\left\{ c_j(t), c_j^\dagger(0) \right\}_+ \right\rangle / \mathcal{Z}, \qquad (3)$$

with $\theta(t)$ the unit step function, Tr denoting the trace over all conduction electron and localized electron states of the lattice, $\beta = 1/T$, $c_j(t) = \exp(it\mathcal{H})c_j \exp(it\mathcal{H})$, the braces denote an anticommutator, and $\mathcal{Z} = \mathbf{Tr}\langle \exp(-\beta\mathcal{H}) \rangle$. We chose to evaluate the local Green's function at site j, but it is the same at every site when there is no long range order. In the limit of infinite coordination number, we find that the many-body self energy for the Green's function becomes local[6], and the many-body problem for the lattice can be mapped onto the many-body problem for an impurity in a time-dependent field with a selfconsistency relation to the lattice[8]. The Fourier transform of the retarded Green's function can be determined (on the Bethe lattice) by solving a simple cubic equation[9,10]

$$G^3(\omega) - 2\omega G^2(\omega) + (1 + \omega^2 - \frac{U^2}{4})G(\omega) - \omega = 0, \qquad (4)$$

where one must choose the (causal) physical solution determined by the root with a negative imaginary part (when the imaginary part is nonzero) and by continuity when real. The conduction electron DOS is defined by $A(\omega) = -\text{Im}G(\omega)/\pi$, the electronic self energy (on the Bethe lattice) satisfies

$$\Sigma(\omega) = \omega + \frac{U}{2} - G(\omega) - \frac{1}{G(\omega)}, \qquad (5)$$

and the dynamical mean field $\lambda(\omega)$ is defined to satisfy

$$G(\omega) = \frac{1}{\omega + \frac{U}{2} - \lambda(\omega) - \Sigma(\omega)} \qquad (6)$$

which can be thought of as the Fourier transform of the time-dependent field for the impurity problem (indeed the dynamical mean-field theory approach is to construct an impurity problem in a time-dependent λ field and then adjust the field until the Green's functions for the impurity are equal to the local Green's functions for the lattice[8]).

In order to calculate the f-electron Green's function, we must first start with the impurity problem, whose Hamiltonian is the same as the lattice Hamiltonian, but there is no hopping term, since it is restricted to the single site of the impurity. The hopping of the conduction electrons is mimicked by the time dependent A field which destroys a conduction electron at time 0 and creates a conduction electron at time t with "strength" $\lambda(t)$. The (greater) f-electron Green's function is then defined by

$$G_f^>(t) = -\mathbf{Tr}\left\langle e^{-\beta\mathcal{H}_{imp}} S_c(\lambda) f(t) f^\dagger(0) \right\rangle / \mathcal{Z}_{imp}, \qquad (7)$$

with $f(t) = \exp(it\mathcal{H}_{imp}) f \exp(-it\mathcal{H}_{imp})$ and the evolution operator given by

$$S_c(\lambda) = \mathcal{T}_c \exp\left[\int_c d\bar{t} \int_c d\bar{t}' c^\dagger(\bar{t}) \lambda_c(\bar{t}, \bar{t}') c(\bar{t}') \right]. \qquad (8)$$

The time-ordering is along the Keldysh contour (see Figure 1), and the contour-ordered dynamical mean field is found from a Fourier transform of $\lambda(\omega)$

$$\lambda_c(\bar{t}, \bar{t}') = -\frac{1}{\pi} \int_{-\infty}^{\infty} d\omega \, \text{Im} \, \lambda(\omega) \exp\left[-i\omega(\bar{t} - \bar{t}') \right]$$

$$\times \left[f_{FD}(\omega) - \theta(\bar{t} - \bar{t}') \right], \qquad (9)$$
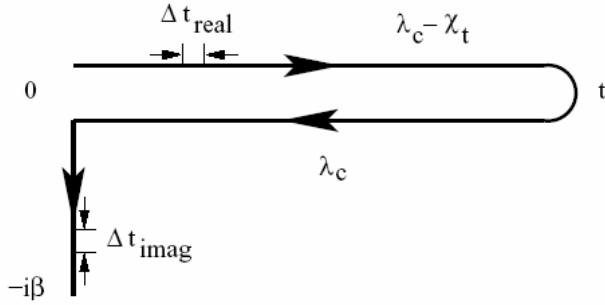
Figure 1. Keldysh contour for evaluating the *f*-electron Green's function at time *t*. The contour runs from $\bar{t} = 0$ to $\bar{t} = t$, then back from $\bar{t} = t$ to $\bar{t} = 0$ and finally goes along the imaginary axis down to $\bar{t} = -i\beta$. The field $\lambda_c - \chi_t$ is active on the forward branch, and the field λ_c is active over the backward branch and the imaginary branch. When we discretize the matrix operator over the Keldysh contour, we evaluate the integrals via a rectangular (midpoint) summation with a step size of Δt_{real} on the real axis and Δt_{imag} on the imaginary axis. We choose $\Delta t_{imag} = 0.05$ and vary Δt_{real} from 0.1 to 0.0125 in our calculations. We typically use no more than 1000 time steps on the outward branch of the contour.

where $f_{FD}(\omega) = 1/[1+\exp(\beta\omega)]$ is the Fermi-Dirac distribution and $\theta_c(\bar{t} - \bar{t}') = 0$ if $\bar{t}'$ is in front of $\bar{t}$ on the contour *c* and 1 if it is behind.

This Green's function can be solved directly by evaluating a Feynman path integral over the Keldysh contour to yield[11,7]

$$G_f^>(t) = -\frac{e^{iUt/2}+e^{\beta U/2-iUt/2}}{\mathcal{Z}_{imp}}$$

$$\times \text{Det}\left[\delta_c(\bar{t} - \bar{t}') + \int_c d\bar{t}'' g^{aux}(\bar{t},\bar{t}')\lambda(\bar{t}',\bar{t}'')\right] \quad (10)$$

which involves the determinant of a continuous matrix operator (note the path integral is the time-ordered product along the integration contour, which is the Keldysh contour here). The function g^{aux} appears in Table 1. It is the Green's function for a noninteracting Fermion that evolves in a time-dependent field $\chi_t(\bar{t},\bar{t}') = iU\theta_c(t-\bar{t})\delta_c(\bar{t} - \bar{t}')$, which arises from the time dependence of the localized electron[11,7]. In this sense, one has the fields $\lambda_c - \chi_t$ acting on the forward branch of the Keldysh contour, and the field λ_c acting on the backward and imaginary branches of the contour. The (equilibrium) greater Green's function satisfies a spectral formula with the DOS and the Fermi-Dirac distribution function (because the equilibrium distribution function is known)

$$G_f^>(t) = \int_{-\infty}^{\infty} d\omega e^{-i\omega t}\left[f_{FD}(\omega)-1\right]A_f(\omega). \quad (11)$$

Table 1. $g^{aux}(\bar{t}, \bar{t}')$ for different orderings of $t, \bar{t}$ and $\bar{t}'$ along the contour *c*. the symbol $\bar{\xi}_0$ satisfies $\bar{\xi}_0 = 1/\left[1 + \exp(iUt - \beta U2)\right]$.

Green's function value	Domain
$\xi_0\exp\left[iU\left(\bar{t} - \bar{t}'\right)/2\right]$	$t < \bar{t} < \bar{t}'$
$\xi_0\exp\left[iUt - iU\left(\bar{t} - \bar{t}'\right)/2\right]$	$\bar{t} < t < \bar{t}'$
$\xi_0\exp\left[-iU\left(\bar{t} - \bar{t}'\right)/2\right]$	$\bar{t} < \bar{t}' < t$
$(\bar{\xi}_0 - 1)\exp\left[iU\left(\bar{t} - \bar{t}'\right)/2\right]$	$t < \bar{t}' < \bar{t}$
$(\bar{\xi}_0 - 1)\exp\left[-iUt + iU\left(\bar{t} + \bar{t}'\right)/2\right]$	$\bar{t}' < t < \bar{t}'$
$(\bar{\xi}_0 - 1)\exp\left[-iU\left(\bar{t} - \bar{t}'\right)/2\right]$	$\bar{t}' < \bar{t} < t$

Using the fact that the greater Green's function satisfies $G_f^>(t) = G_f^{>*}(-t)$ and the fact that the DOS at half filling is an even function of ω (due to particle-hole symmetry) yields the final equation for the *f*-electron DOS[11,7]

$$A_f(\omega) = -\frac{2}{\pi}\int_0^{\infty} dt\text{Re}\left\{G_f^>(t)\right\}\cos(\omega t). \quad (12)$$

In addition to computing the Green's function on the real frequency axis, one can also compute it on the imaginary (Matsubara) frequency axis, at the Matsubara frequencies $i\omega_n = i\pi T(2n + 1)$. In this case, one can formulate the expressions as the determinant of a discrete matrix, so there is no error associated with discretizing a continuous matrix operator[11,7]. Since the Matsubara Green's function can also be expressed as an integral over the DOS

$$G_f(i\omega_n) = \int d\omega \frac{1}{i\omega_n - \omega}A_f(i\omega), \quad (13)$$

we have an independent way to verify the accuracy of the DOS by comparing the integral formula for $G(i\omega_n)$ with the result directly calculated on the imaginary axis. Usually the accuracy is worst for the lowest Matsubara frequency.

There also are a number of moments and properties of the DOS that can be tested. First, the DOS is always nonnegative—negative values of the DOS for some region of frequency indicate an error in the calculations. Second, one can work out explicit values for the first three moments. At half filling, these satisfy

$$\int d\omega A_f(\omega) = 1, \qquad (14)$$

$$\int d\omega A_f(\omega) \omega f_{FD}(\omega) = U\left(\left\langle c^\dagger c f^\dagger f \right\rangle - \frac{1}{4}\right), \qquad (15)$$

$$\int d\omega A_f(\omega) \omega^2 = \frac{U^2}{4}. \qquad (16)$$

In practice we add a small shift (always less than 0.006 in magnitude) to the DOS in order to satisfy the unit weight sum rule (Eq. 14). Then we check the accuracy of the other two sum rules [by independently calculating the correlation function on the right hand side of Eq. (15)]. At $t = 0$, we can use the moments in (Eqs. 14–16) to show that

$$G_f^>(0) = -\frac{1}{2}, \qquad (17)$$

$$\frac{d}{dt} G_f^>(0) = -iU\left(\left\langle c^\dagger c f^\dagger f \right\rangle - \frac{1}{4}\right), \qquad (18)$$

$$\frac{d^2}{dt^2} G_f^>(0) = \frac{U^2}{4}. \qquad (19)$$

Thus the first derivative depends on temperature, but is purely imaginary, while the second derivative is real and independent of T. Hence we expect $\operatorname{Re} G_f^>(t)$ to depend weakly on T for small times, and to show stronger dependence at large times.

3. Computational Algorithm

The main effort of this nonequilibrium calculation is to compute the f-electron Green's function, which requires the determinant of the continuous matrix operator in Eq. 10. To calculate this, we must first decide on a discretization along the contour to evaluate line integrals over the contour (see Figure 1). Our choice is to use a step size of Δt_{real} on the real axis and $\Delta t_{\text{imag}} = 0.05$ along the imaginary axis. We use a midpoint rectangular integration rule, evaluating the function at the midpoint of each discretized piece of the contour, for the approximation to the line integral. Hence

$$\int_c d\bar{t} h(\bar{t}) = \sum_j W_j h(\bar{t}_j), \qquad (20)$$

with the weight function W_j satisfying $W_j = \pm\Delta t_{\text{real}}$ on the real axis (positive on the forward branch and negative on the backward branch) and $W_j = -\Delta t_{\text{imag}}$ on the imaginary axis. The times where the function is evaluated are $t_j = (j - 1/2)\Delta t_{\text{real}}$ on the forward branch, $t_j = (2j_{\text{max}} - j + 1/2)\Delta t_{\text{real}}$ on the backward branch, and $_j = (2j_{\text{max}} - j + 1/2)\Delta t_{\text{imag}}$ on

the imaginary branch (j_{jmax} is the number of points on the forward branch of the Keldysh contour). Using this scheme, a Dirac delta function is approximated by

$$\delta_c(\bar{t}_j - \bar{t}_{j'}) = \frac{1}{W_j}\delta_{i,j'}. \qquad (21)$$

The evaluation of a discrete approximation to the determinant of the continuous operator is now a straightforward procedure[11]. First we note that

$$\operatorname{Det}_c(1 + M) = \exp\left(\mathbf{Tr}_c\left[\ln\{1 + M\}\right]\right) = \exp\left(\sum_n \frac{1}{n}\mathbf{Tr}_c M^n\right), \qquad (22)$$

is a relation relating to the trace of a series of pwers of the matrix M. The symbol Tr_c denotes the trace of a matrix operator over the Keldysh contour, and it satisfies

$$\mathbf{Tr}_c M = \int_c d\bar{t} M(\bar{t}, \bar{t}) = \sum_i W_i M(t_i, t_i). \qquad (23)$$

Hence the trace of the powers of M becomes

$$\mathbf{Tr}_c M^n = \sum_{i_1 \ldots i_1} W_{i_1} \ldots W_{i_n} M(t_{i_1}, t_{i_2}) \ldots M(t_{i_n}, t_{i_1}). \qquad (24)$$

Now we define a new discrete matrix to satisfy $\bar{M}(t_i, t_j) = W_i M(t_i, t_j)$. Then we find the trace in Eq. (24) becomes

$$\mathbf{Tr}_c M^n = \sum_{i_1 \ldots i_1} W_{i_1} \ldots W_{i_n} M(t_{i_1}, t_{i_2}) \ldots M(t_{i_n}, t_{i_1}), \qquad (25)$$

and leads to the final formula for the determinant

$$\operatorname{Det}_c\left(1 + M\right) = \operatorname{Det}\left(1 + \bar{M}\right), \qquad (26)$$

which approximates the determinant of the continuous matrix operator defined over the Keldysh contour by a matrix determinant of the discrete matrix $1 + \bar{M}$. Hence, for each value of t that we wish to calculate the f-electron Green's function, we must first generate the corresponding matrix $1 + \bar{M}$ for the Keldysh contour that runs out to time t and then take its determinant. Since the matrix can be generated solely from the parameters $U, t, T,$ and $.\lambda(\omega)$, this algorithm is easily parallelized. We first generate the function $\lambda(\omega)$ on a discrete real frequency grid [by solving for the conduction electron Green's function, Eq. 4, on the master node, and then send that data to all of the slave nodes of the parallel process. Each slave process calculates the relevant matrix (which is a general complex matrix, with no special symmetries or properties), diagonalizes the matrix to find its eigenvalues, and then computes the determinant by taking a product of the eigenvalues. This is then sent back to the master who computes $G_f^>(t)$ from Eq. 10 and sends a new value of t to the slave to continue the computation. The algorithm has essentially a linear scale up in the parallelization, and it is quite efficient, since the

limiting step is the diagonalization of the matrix, which is optimized by the local implementation of LAPACK and BLAS on the given parallel computer. We perform the majority of our calculations on a Cray T3E, which limits the matrix sizes to approximately 2100×2100 on a 256 MEG node, and we can increase the matrix size slightly when working on higher memory nodes, but the diagonalization time then becomes a limiter, if it takes longer than the queue limits for those nodes on a given machine.

We fix the grid spacing on the imaginary axis, since we find the results are not too sensitive to changes of the step size there, and the value $\Delta t_{\text{imag}} = 0.05$ is sufficient for our purposes. On the real time axis, we generally take Δt_{real} to vary from 0.1 down to 0.0 125. But since the calculations at different values of t are completely independent of one another, we do not need to use the same grid spacing of the t-values for which we compute $G_f^>(t)$. We find that choosing a real time axis spacing of 0.2 or 0.1 [for generating the data for $G_f^>(t)$] is usually sufficiently accurate. We perform an Akuba shape preserving spline and evaluate the splined Green's function on a grid of size 0.01 or 0.005 before evaluating the cosine Fourier transform in Eq. 12. This allows the accuracy to improve for larger frequency values, without producing a significant increase in computational time. Finally, the results of the Fourier transform, especially at small frequencies, depend on the cutoff or maximal time value where $G_f^>(t)$ is evaluated. Since the Green's function decays at large times, imposing a cutoff is like replacing the Green's function by 0 for times larger than the cutoff. We find that this usually causes no significant errors to the calculations when the maximum value of the Green's function is less than approximately 10^{-4} to 10^{-5} in magnitude at the point where the cutoff is imposed.
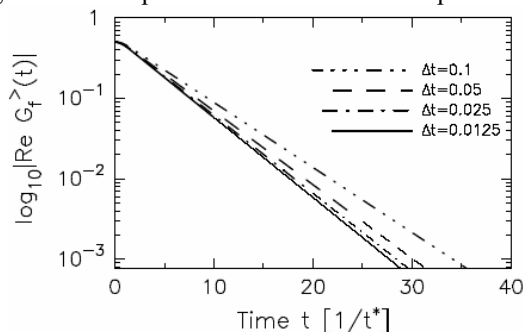

Figure 2. Logarithm of the absolute value of $G_f^>(t)$ for $U = 1$ and $T = 5$. We plot results for Δt_{real} l = 0.1, 0.05, 0.025, and 0.0125. Note how the Green's function has a simple exponential decay at large times, and how the decay constant depends on the discretization size. The thick curves are the calculated data, and the thin curves are the extrapolated results.

4. Numerical Results

When $U = 0$, the system is noninteracting, and the f-electron DOS is a delta function for all temperatures. When U increases, the f-electron DOS broadens into a regular function and picks up T-dependence (surprisingly, the conduction electron DOS is always independent of temperature[10]). For small values of U, we expect the low-temperature f-electron Green's function to be a sharply peaked function with unit weight. The Fourier transform of this function to the real axis, will then be an exponentially decaying function, with a slower decay for a more sharply peaked function. Hence, we expect the greater Green's function to have an exponential tail for large times. At small times, the Green's function approaches $\rho_f = 1$ for all temperatures, and the curves for different temperatures start to separate only for larger times.

We illustrate the output of our calculations for the case $U = 1$ and $T = 5$ in Figure 2. We plot the logarithm of the absolute value of the real part of $G_f^>(t)$ for four different choices of Δt_{real}. We find, in all cases, that the Green's function has an exponentially decaying behavior at large times, so we append an exponential function out to large times, in order to have the Green's function smaller than 10^{-4} at the maximal t cutoff. The extrapolated curves are represented by the thin lines. Note how there is a clear dependence of the Green's function on the step size taken along the real axis. Since this is a semi-log plot, it suggests that one extrapolate the logarithm of $G_f^>(t)$ to determine the $\Delta t_{\text{real 1}} \to 0$ limit. But this procedure becomes problematic once the Green's function crosses zero, or has oscillatory behavior in the tails, so we do not carry out such a procedure here (note one might have expected $G_f^>(t)$) to have a quadratic dependence on $\Delta t_{\text{real 1}}$ due to a Trotter formula, but that does not apply here, since there is no simple Trotter breakup of the continuous matrix operator we are computing the determinant of).

Next we examine the same set of parameters, but at lower temperature $T = 0.15$ in Figure 3. Here the dependence on the discretization size is much stronger, with the exponential decay quite slow for the largest Δt_{real}. This shows that the discretization size needs to be reduced as T is reduced, making lower temperature calculations much more difficult than higher temperature. Also, the maximal cutoff in time needs to be pushed farther out, unless one can append an extrapolated functional form (as we do here) for large times.
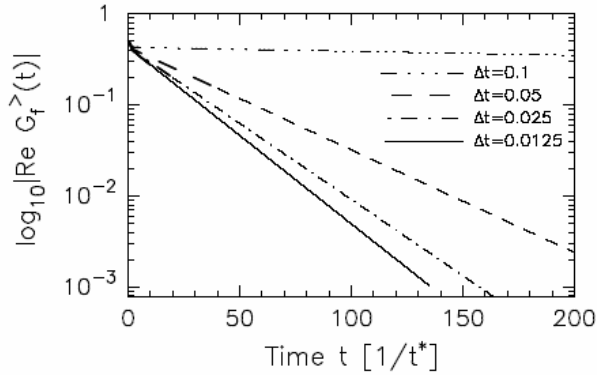
Figure 3. Logarithm of the absolute value of $G_f^>(t)$ for U = 1 and T = 0.15. We plot results for Δt_{real} = 0.1, 0.05, 0.025, and 0.0125. Note how he Green's function has a simple exponential decay at large times, and how the decay constant depends strongly on the discretization size. The thick curves are the calculated data, and the thin curves are the extrapolated results.

The next step is to perform the Fourier transform (after splining the time data) as in Eq. 12. We can then take the data for the DOS for different Δt_{real} values and try to perform a pointwise (in ω) extrapolation down to Δt_{real} = 0. Since we do not know how the curves depend on Δt_{real}, we use an n-point Lagrange interpolation formula, which is a linear extrapolation for n = 2, a quadratic extrapolation for n = 3 and a cubic extrapolation for n = 4. By checking the different sum rules and the values of the Green's function at the Matsubara frequencies, we can examine the accuracy of different extrapolation schemes. Sometimes it is better to use all of the data and a large n Lagrange extrapolation scheme. Other times, the large step-size error is so big, that that data is not trustworthy, and it is more accurate to use an extrapolation with just the smaller discretization sizes (usually a linear extrapolation method with the smallest two values of Δt_{real} is used). We call this extrapolation technique the δ-extrapolation.

Often, we find that the exact value for the Green's function at the lowest Matsubara frequency lies in between the value for the smallest Δt_{real} and the value generated from the δ -extrapolation. In this case, we usually can improve the DOS if we perform a second extrapolation, averaging those two DOS to produce the correct value for $G_f(i\omega_0)$. We call this extrapolation scheme Matsubara-extrapolation.

To illustrate how the extrapolation procedures work, we first examine the high-temperature case T = 5. The results for the DOS for the four different discretization sizes and for the δ-extrapolation is shown in Figure 4. It is apparent from the figure that the DOS broadens and the peak is reduced as the discretization size is made smaller.

The δ extrapolation uses the two smallest values of Δt_{real} and a linear extrapolation (we found that gave the most accurate results). A summary of the moment sum rules and the spectral formula for the Matsubara Green's functions is given in Table 2. It is clear from that data that a systematic extrapolation is possible, and that the final result is highly accurate for the DOS (errors are less than 0.1 % for the first moment, 0.03% for the second moment, and 0.003% for the lowest Matsubara frequency). It is hard to judge the absolute accuracy of the DOS from these integrated sum rules, but as a general rule, if the moment sum rules are accurate to better than 1 % and the Matsubara frequency Green's functions are accurate to better than 0.1 %, then the DOS has an absolute accuracy that is probably better than a few percent for most frequencies, except those near the tails, where the DOS is small and may even go negative.
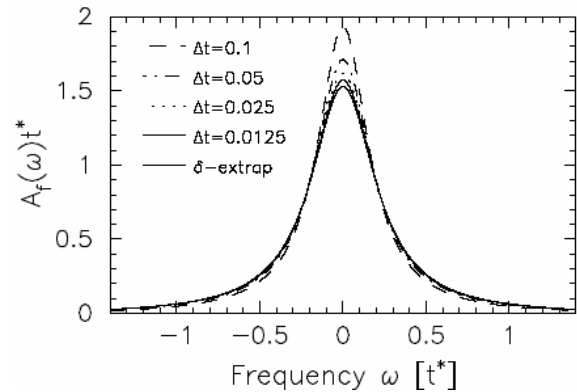

Figure 4. DOS for U = 1 and T = 5 and different values of Δt_{real}. Also plotted is the result of the δ-extrapolation. One can see clearly that the DOS is converging to a well-defined limit as the discretization error is reduced.

Table 2. Summary of moment sum rules and the matsubara green'sfunction for the case U = 1 and T = 5. The first four rows are different values of otreal. The last row is the exact result. Shift is the value added to the dos to satisfy the sum rule in Eq. 14.

Case	Eq. 15	Eq. 16	$G_f(i\omega_0)$	shift
0.1	−0.00787	0.15805	−0.063667	0.00484
0.05	−0.00991	0.19933	−0.063660	0.00500
0.025	−0.01087	0.21863	−0.063628	0.00253
0.0125	−0.01137	0.22873	−0.063623	0.00125
δ-extrap.	−0.01241	0.25007	−0.063600	−10−6
Exact	−0.01240	0.25	−0.063598	0.0

We next examine the low-temperature case of U = 1 and T = 0.15 in Figure 5. Note how the large Δt_{real} case has an extremely narrow DOS, and how the DOS broadens dramatically as the step size is reduced. We are able to make this reduction, since we can append the

exponential tail out to large times, which allows us to perform the relevant Fourier transforms. We plot two extrapolation techniques: the δ-extrapolation, using a linear extrapolation with the two smallest step sizes (since that is the most accurate), and the Matsubara-extrapolation procedure, which averages the Δt_{real} = 0.0125 DOS with the δ-extrapolated DOS in order to properly reproduce the lowest Matsubara frequency Green's function. Since the δ-extrapolated result overshoots the correct answer, this averaging procedure significantly enhances the results. Even so, one can see from Table 3 that the errors are much larger at low temperature than at high temperature (this was already apparent from Figure 3). The error in the moment from Eq. 15 is 1%, the moment from Eq. 16 is 1.5% and for the Matsubara frequency Green's function $G_f(i\omega_1)$ is 0.07%.
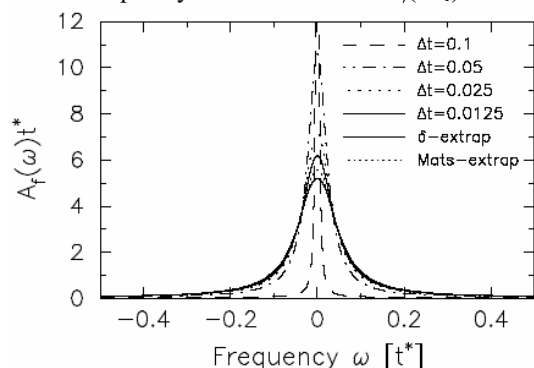

Figure 5. DOS for U = 1 and T = 0.15 and different values of Δt_{real}. Also plotted is the result of the δ-extrapolation and the Matsubara-extrapolation. One can see that the DOS is converging to a well-defined limit as the discretization error is reduced, but the accuracy is significantly reduced relative to the higher temperature case in Figure 4.

Hence these calculations become significantly more challenging as the temperature is lowered. To understand the thermal evolution of the f-electron DOS, we summarize data collected for a number of different temperatures in Figure 6. In addition, we plot the temperature-independent conduction electron DOS with the magenta dashed line. Note how the conduction electron DOS is rather broad, but the f-electron DOS becomes sharply peaked at low temperature. By scaling the results to T = 0, we conjecture that the maximum of the f-electron DOS approaches 21 as $T \to 0$. As the DOS becomes more sharply peaked, we need to have a transfer of some spectral weight to larger energy as well ($|\omega|>1.5$), since the second moment sum rule in Eq. 16 is independent of temperature, and as the peak grows in height, it contributes less to that sum rule. There is an interesting contrast in the DOS of the two different particles. The conduction electron DOS is broad and does not evolve with temperature, while the f-electron DOS has

strong temperature dependence becoming sharply peaked at low temperature and weak coupling. By carefully performing extrapolations of the exponential decay of the greater Green's function at large time and of the discretization error of the DOS, we can produce accurate results for the f-electron DOS. The calculational needs can easily go beyond computational resources at low temperature, though.

Table 3. Summary of moment sum rules and the Matsubara Green's function for the case U = 1 and T = 0.15. The first four rows are different values of Δt_{real}. The last row is the exact result.

Case	Eq. 15	Eq. 16	$G_f(i\omega_0)$	$G_f(i\omega_1)$
0.1	−0.05361	0.12596	−1.194404	−0.6832
0.05	−0.08145	0.20057	−1.185551	−0.6742
0.025	−0.09030	0.21792	−1.181501	−0.6694
0.0125	−0.09760	0.24410	−1.179435	−0.6668
δ-extrap.	−0.10370	0.25936	−1.177368	−0.6642
M-extrap.	−0.10112	0.25390	−1.78105*	−0.6651
Exact	−0.10217	0.25	−1.78106	−0.6656

Next we focus on the strong-coupling regime with U = 5. In this case, the conduction electron DOS has a correlation induced gap from the Mott transition, which occurs at U = 2. When the DOS develops a gap at low ω, the greater Green's function has a strong oscillatory component at large times. Unfortunately there does not appear to be any simple rule that could be used to append an extrapolated result to the Green's function at large time. This greatly reduces the ability to calculate accurate results at low temperature, because the discretization size needs to be small, but the cutoff in time needs to be large, and this often goes beyond available computer resources.

In Figure 7, we plot the greater Green's function versus time for T = 1. In panel (a), the short-time results are shown—note how the curves for different discretization size lie almost on top of each other. In panel (b), we show the larger time results (the smallest discretization size [green curve] only goes to t = 27). What is interesting to note is that the amplitude of the oscillations is reduced as the discretization size is reduced, but the period remains essentially the same. This might suggest to try to determine the amplitude reduction factor for the limit $\Delta t_{real} \to 0$, and apply that to the curves for finite Δt_{real} to extrapolate to the exact result. The problem is that such a scheme does not work well, as it tends to generate an unphysical peak in the low-frequency DOS, and it produces worse agreement for both the moments and the Matsubara Green's functions, so we don't discuss that scheme further.
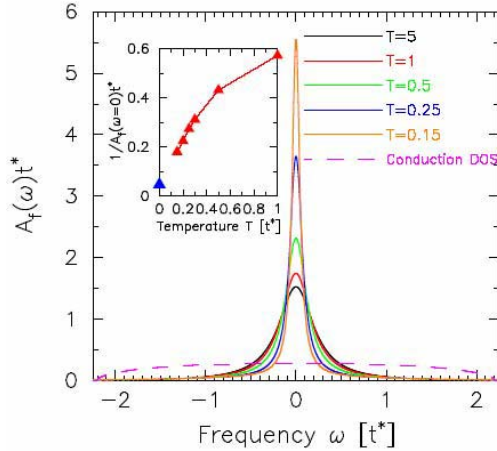
Figure 6. Summary plot for the *f*-electron DOS for *U* = 1 and a number of different temperatures. The magenta dashed line is the conduction electron DOS (which is independent *of* temperature). Inset is a plot *of* 1/$A_f(\omega = 0)$ versus *T*, to extrapolate the DOS down to *T* = 0. We predict that the DOS grows to a peak height of about 21 at *T* = 0 (blue triangle in inset).
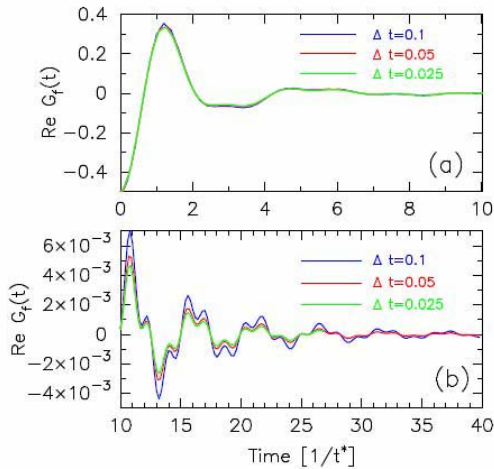

Figure 7. Greater Green's function for *U* = 5 and *T* = 1 for different Δt_{real}. Panel (a) is the short-time results and panel (b) is the longer-time results. Note how the curves are virtually identical for short times, but there is a systematic reduction in the amplitude of the oscillations as Δt_{real}, is reduced.

We are thus left with using the same δ and Matsubara extrapolation schemes that we used for the small-U case. At high temperature, everything works out reasonably well, as can be seen in Table 4. But we do not achieve anywhere near as high an accuracy as for small *U*. When we go to lower temperatures, the accuracy becomes worse, and there is limited improvement from the extrapolation schemes. This occurs because when the discretization size is too large, the DOS becomes negative in the gap region, while when the size is small enough to

correct the DOS in the gap region, it suffers from Gibb's oscillations due to the sharp cutoff in time, since the cutoff is not large enough for an accurate Fourier transform. These results are summarized in Figure 8 and Table 5. Note that the sum rules do not change much as the DOS varies in the gap region, because the overall DOS is small and because we multiply by powers of w which suppress the weight in the integral from the gap region.
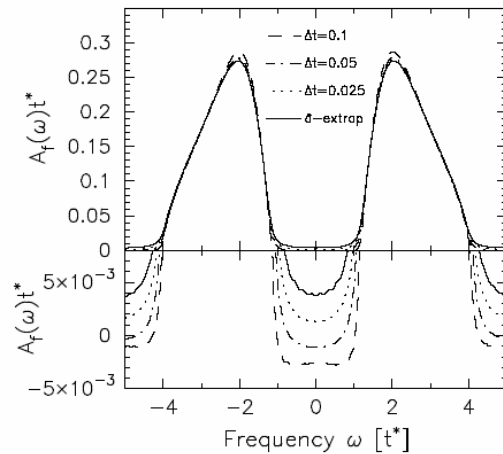

Figure 8. DOS for *U* = 5 and *T* = 1. Three different values of Δt_{real} and the b extrapolation are shown. In the lower panel, the vertical axis of the figure is blown up to highlight that the DOS in the gap region is negative for large discretizations and becomes positive only as the discretization is reduced.

Table 4. Summary of moment sum rules and the Matsubara Green's function for the case *U* = 5 and *T* = 5. The first two rows are different values of Δt_{real}. The last row is the exact result. Shift is the value added to the DOS to satisfy the sum rule in Eq. 14.

Case	Eq. 15	Eq. 16	$G_f(i\omega_0)$	shift
0.1	−0.30191	6.19393	−0.062162	0.00486
0.05	−0.30299	6.21921	−0.062147	0.00502
δ-extrap.	−0.30396	6.24237	−0.062120	0.00010
Exact	−0.30422	6.25	−0.062101	0.0

Finally, a summary of the DOS data for *U* = 5 is plotted in Figure 9. We see that there is significant subgap DOS at high temperature, which is reduced as *T* is lowered. We also see the peak in the *f*-electron DOS move towards the band edge as *T* is lowered. Finally, it appears that the *f*-electron DOS and the conduction electron DOS will both share the same bandwidth at *T* = 0. We are severely limited by how low we can go in temperature and still maintain positive DOS in the gap region.

Table 5. Summary of moment sum rules and the Matsubara Green's function for the case $U = 5$ and $T = 1$. The first three rows are different values of Δt_{real}. The last row is the exact result. Shift is the value added to the DOS to satisfy the sum rule in Eq. 14.

Case	Eq. 15	Eq. 16	$G_f(i\omega_0)$	shift
0.1	−1.01562	6.28460	−0.203553	0.00504
0.05	−1.01334	6.30267	−0.203146	0.00507
0.025	−1.01012	6.29576	−0.202731	0.00504
δ-extrap.	−1.00095	6.30842	−0.202735	−0.00315
Exact	−0.00177	6.25	−0.203916	0.0

5. Conclusions and Outlook

In this contribution, we have presented a summary of numerical calculations employing a nonequilibrium formalism over the so-called Keldysh contour. The calculations involve determining the determinant of a continuous matrix operator defined along the Keldysh contour, which is found by calculating the determinant of a discretized version of the operator, which is a general complex matrix, defined differently for each value of time. This formalism is easily parallelized, is efficient on each node, and has nearly linear scale-up. We examined the simplest problem with this numerical algorithm—the *f*-electron spectrum of the Falicov-Kimball model. This problem is useful because a number of sum rules exist, that allow one to determine the accuracy of the calculations.

Our results show that one needs to carefully perform an analysis of the dependence of the solutions on the discretization along the Keldysh contour. Sometimes results can be extrapolated to the continuum limit, other times, this is not possible. We also find that these results often require a finer discretization at lower temperature. We anticipate similar numerical issues will arise in other nonequilibrium problems that employ the same formalism.

These results provide useful benchmarks for more interesting nonequilibrium problems such as the interaction of a strongly correlated material with a strong external electromagnetic field or the nonlinear response of an inhomogeneous multilayered device to an external voltage (including a noise analysis of the current). These latter problems are likely to have more of an applied interest to the military. The calculational formalism needs to be generalized for each of these cases. One needs to find a way to self-consistently map an impurity or cluster problem onto the lattice problem (in the presence of the time-dependent field), and then perform similar computations along the Keldysh contour. The impurity-like problems are similar, but we need to perform a summation over the lattice wave vector (which

can be represented by a double integral over a generalized joint density of states for each matrix element of the contour-ordered Green's function) to complete the self-consistent algorithm. Far fewer sum rules will exist to benchmark the results, so an analysis in terms of scaling with respect to the discretization size will need to be performed. One can check the nonequilibrium results in the linear-response regime with the results of Kubo-formula-based approaches, which will provide a stringent test of the quality of the numerics.
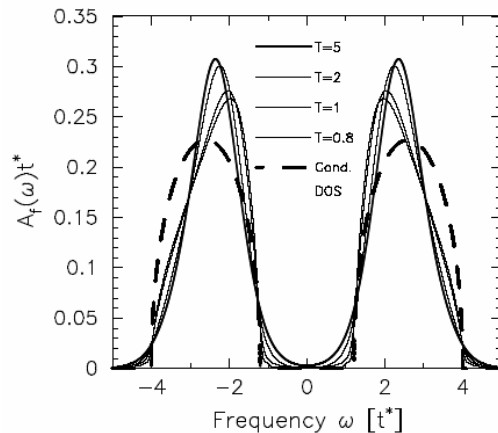
Figure 9. Summary DOS for $U = 5$. The data for $T = 5$ comes from the δ-extrapolation, for $T = 2$ from $\Delta t_{real} = 0.05$, and the lower temperatures have $\Delta t_{real} = 0.025$. We also include the conduction electron DOS with the dashed line. Note how the subgap DOS for the *f*-electron decreases as T is lowered, and how the DOS moves more towards the band edge as T is reduced. We also see the large $|\omega|$ DOS start to pinch off at the conduction electron DOS band edge as T is lowered. We expect the bandwidths of both the conduction and *f*-electrons to be equal at $T = 0$. The oscillations apparent in the $T = 0.8$ data are an artifact of a time-domain cutoff that is too short.

Acknowledgments

References

1. Josephson, B.D., "Possible new effects in superconductive tunneling." *Phys. Lett*, 1, 1962, pp. 251–255.

2. Mukhanov, O.A., V.K. Semenov, and K.K. Likharev, "Ultimate performance of the RSFQ logic circuits." *IEEE Trans.*

Magn. Mate.," MAG-23, 1987, pp. 759–762; Likharev, K.K., "Superconductor devices for ultrafast computing." in *Applications of Superconductivity*, Ed. by Weinstock, H. (Kluwer, Dordrecht, 2000), Ch. 5.

3. Keldysh, L.V., "Diagram Technique for Nonequilibrium Processes." *J. Exptl. Theoret. Phys.*, 47, 1964*,* pp. 1515–1520, [*Sov. Phys. JETP*, 20, 1965, pp. 1018–1022].

4. Rammer, J. and H. Smith, "Quantum field-theoretical methods in transport theory of metals." *Rev. Mod. Phys.*, 58, 1986, pp. 323–359.

5. Falicov, L.M. and J.C. Kimball, "Simple model for semiconductor metal transitions: SmB_6 and transition-metal oxides." *Phys. Rev. Lett.*, 22,1969, pp. 997–999.

6. Metzner, W. and D. Vollhardt, "Correlated Lattice Fermions in $d = \infty$ Dimensions." *Phys. Rev. Lett.*, 62, 1989*,* pp. 324–327.

7. Freericks, J.K. and V. Zlatić, "Exact dynamical mean field theory of the Falicov-Kimball model." *Rev. Mod. Phys.*, 75, 2003*,* pp. 1333–1382.

8. Brandt, U. and C. Mielsch, "Thermodynamics and correlation functions of the Falicov-Kimball model in large dimensions." *Z. Phys. B–Condens. Mat.*, 75, 1989, pp. 365–370; "Thermodynamics of the Falicov-Kimball model in large dimensions II." *Z. Phys. B-Condens. Mat.*, 79,1990*,* pp. 295–299.

9. Hubbard, J. "Electron correlations in narrow energy bands 111. An improved solution." *Proc. R. Soc. (London) See A*, 281, 1965, pp. 401–419.

10. Van Dongen, P.G.J. "Exact mean-field theory of the extended simplified Hubbard model." *Phys. Rev. B*, 45, 1992, pp. 2267–2281; Van Dongen, P.G.J. and Leinung, C., "Mott-Hubbard transition in a magnetic field." *Ann. Phys.*, 6, 1997, pp. 45–67.

11. Brandt, U. and M.P. Urbanek, "The *f*-electron spectrum of the spinless Falicov-Kimball model in large dimensions." *Z. Phys. B-Condens. Mat.*, 89, 1992, pp. 297–303.